
Massive star formation in the Carina nebula complex and Gum 31 – II. a cloud–cloud collision in Gum 31

Shinji FUJITA^{1*}, Hidetoshi SANO², Rei ENOKIYA³, Katsuhiro HAYASHI⁴, Mikito KOHNO⁵, Kisetsu TSUGE⁶, Kengo TACHIHARA⁷, Atsushi Nishimura⁸, Akio OHAMA⁷, Yumiko YAMANE⁷, Takahiro OHNO⁷, Rin I. YAMADA⁷ and Yasuo FUKUI⁷

¹Department of Physical Science, Graduate School of Science, Osaka Prefecture University
1-1 Gakuen-cho, Naka-ku, Sakai, Osaka 599-8531, Japan

²National Astronomical Observatory of Japan, Mitaka, Tokyo, 181-8588, Japan

³Department of Physics, Institute of Science and Technology, Keio University, 3-14-1 Hiyoshi,
Kohoku-ku, Yokohama, Kanagawa 223-8522, Japan

⁴Institute of Space and Astronautical Science (ISAS) Japan Aerospace Exploration Agency
(JAXA), 3-1-1 Yoshinodai, Chuo-ku, Sagami-hara, Kanagawa 252-5210, Japan

⁵Astronomy Section, Nagoya City Science Museum, 2-17-1 Sakae, Naka-ku, Nagoya, Aichi
460-0008, Japan

⁶Dr. Karl Remeis Observatory, Erlangen Centre for Astroparticle Physics,
Friedrich-Alexander-Universität Erlangen-Nürnberg, Sternwartstraße 7, 96049 Bamberg,
Germany

⁷Department of Astrophysics, Nagoya University, Furo-cho, Chikusa-ku, Nagoya, Aichi,
464-8602, Japan

⁸Institute of Astronomy, the University of Tokyo, 2-21-1 Osawa, Mitaka, Tokyo 181-0015,

Japan

*E-mail: fujita@p.s.osakafu-u.ac.jp

Received (reception date); Accepted (acceptation date)

Abstract

We present the results of analyses of the ^{12}CO ($J=1-0$), ^{13}CO ($J=1-0$), and ^{12}CO ($J=2-1$) emission data toward Gum 31. Three molecular clouds separated in velocity were detected at -25 , -20 , and -10 km s^{-1} . The velocity structure of the molecular clouds in Gum 31 cannot be interpreted as expanding motion. Two of them, the -25 km s^{-1} cloud and the -20 km s^{-1} cloud, are likely associated with Gum 31, because their ^{12}CO ($J=2-1$)/ ^{12}CO ($J=1-0$) intensity ratios are high. We found that these two clouds show the observational signatures of cloud–cloud collisions (CCCs): a complementary spatial distribution and a V-shaped structure (bridge features) in the position–velocity diagram. In addition, their morphology and velocity structures are very similar to the numerical simulations conducted by the previous studies. We propose a scenario that the -25 km s^{-1} cloud and the -20 km s^{-1} cloud were collided and triggered the formation of the massive star system HD 92206 in Gum 31. This scenario can explain the offset of the stars from the center and the morphology of Gum 31 simultaneously. The timescale of the collision was estimated to be ~ 1 Myr by using the ratio between the path length of the collision and the assumed velocity separation. This is consistent with that of the CCCs in Carina Nebula Complex in our previous study.

Key words: ISM: clouds — ISM: individual objects (Carina) — radio lines: ISM

1 Introduction

Many recent observational studies of star forming region have revealed the triggering of massive star formations via cloud–cloud collisions (CCCs). The two observational signatures—the complementary spatial distributions and bridging features between the colliding clouds—have been suggested as evidence (e.g., Fukui et al. 2021). Such evidence was detected in CCC regions both in the Galactic (e.g., Furukawa et al. 2009; Ohama et al. 2010; Fukui et al. 2014; Torii et al. 2015; Fukui et al. 2016; Fujita et al. 2021a; Fukui et al. 2017a; Torii et al. 2017a; Torii et al. 2017b; Enokiya et al. 2018; Hayashi et al. 2018; Kohno et al. 2018; Nishimura et al. 2018; Sano et al. 2018; Fujita et al.

2021b; Fujita et al. 2019; Fukui et al. 2019; Torii et al. 2021; Torii et al. 2018b; Fukui et al. 2021; Fujita et al. 2021c) and extragalactic (e.g., Tokuda et al. 2019; Sano et al. 2021) objects.

In Fujita et al. (2021c) (hereafter Paper I), we analysed a CO dataset towards the Carina Nebula Complex (CNC). Four discrete molecular clouds at velocities -27 , -20 , -14 , and -8 km s $^{-1}$ were found. Most of them might be associated with the star clusters in the CNC, because their ^{12}CO ($J=2-1$)/ ^{12}CO ($J=1-0$) intensity ratios are high and their distributions correspond to the *Spitzer* 8- μm distributions. In addition to this, we found that these clouds show the observational signatures of a CCC. Furthermore, we also found that the SiO emission (a tracer of a shocked molecular gas) is significantly enhanced between the colliding clouds. For these results, we propose a scenario that the formation of massive stars in the clusters in the CNC was triggered by CCCs with a timescale of ~ 1 Myr.

In this paper, we focus on Gum 31 (E127 in Hanaoka et al. (2019)). Gum 31 located ~ 50 pc from the CNC on the sky plane. The distance to Gum 31 has been discussed and determined to be 2.5 ± 0.3 kpc (Barnes et al. 2010). We adopt the value of 2.5 kpc in this paper. Figure 1(a) shows a composite color image of the WISE 22- μm (red) and *Spitzer*/GLIMPSE 8- μm (green) emissions around Gum 31. It is ionized by the young stellar cluster NGC 3324 (e.g., Walborn 1982) including the double or multiple O-type stars in HD 92206 [HD 92206A at $(l, b) = (286^\circ 223, -0^\circ 170)$, HD 92206B at $(l, b) = (286^\circ 225, -0^\circ 169)$, and HD 92206C (CD-57. $^\circ$ 3378) at $(l, b) = (286^\circ 219, -0^\circ 178)$] (Mathys 1988). Gum 31 is relatively a small and resembles to the *Spitzer* bubbles (Churchwell et al. 2006; Churchwell et al. 2007), although the radius is somewhat larger (~ 10 pc) than is typical for those bubbles. Gum31 is connected to the central parts of the CNC in the Herschel far-infrared maps (Ohlendorf et al. 2013) and CO maps (Yonekura et al. 2005; Rebolledo et al. 2016). In addition, the distance to the CNC is estimated to be ~ 2.3 kpc (e.g., Allen & Hillier 1993; Smith 2006) and thus Gum31 is probably associated with the CNC.

Cappa et al. (2008) investigated the ionized, neutral, and CO gas in the environs of Gum 31 and found that the HI structure is 10.0 ± 1.7 pc in radius, has a neutral mass of $1500 \pm 500 M_\odot$, and is expanding at 11 km s $^{-1}$. They concluded that the expansion of the HII region triggered stellar formation in the molecular shell, although the angular resolution of their CO data is insufficient ($\sim 2'.7$). Detailed gas observations and analyses in such a young [the age of the cluster NGC 3324 is estimated to be < 3 Myr (Carraro et al. 2001)] star forming region are important in revealing the mechanism of massive star formation.

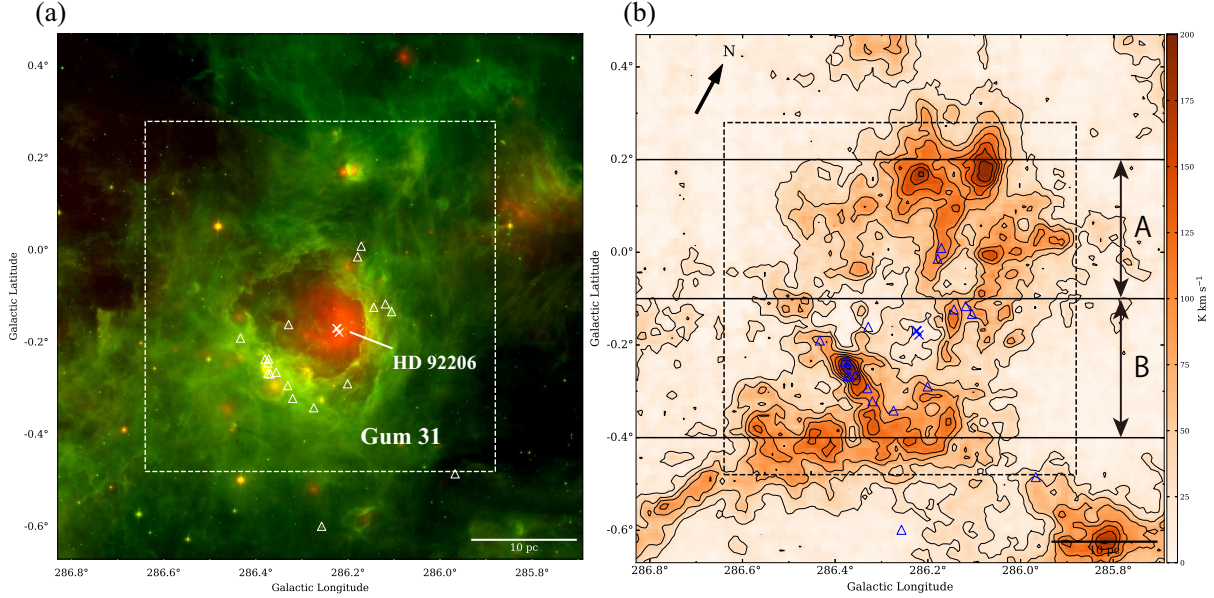


Fig. 1: (a) Composite image of the WISE $22\ \mu\text{m}$ (red) and *Spitzer*/GLIMPSE $8\ \mu\text{m}$ (green) towards Gum 31. (b) The ^{12}CO ($J=1-0$) integrated-intensity map taken from the Mopra archive (Rebolledo et al. 2016; Rebolledo et al. 2017). Integrated velocity range is from -35 to $10\ \text{km s}^{-1}$. The black contours are plotted 25 ($\sim 10\sigma$), 50, 75, ..., $200\ \text{K km s}^{-1}$. The black dotted rectangle indicates the area observed with NANTEN2. The crosses represent the multiple O-stars HD 92206 (Mathys 1988). The triangles represent young stellar objects (Ohlendorf et al. 2013).

2 Dataset

2.1 Mopra

As in Paper I, we used the ^{12}CO and ^{13}CO ($J=1-0$) archived datasets obtained with the Mopra 22-m telescope (Burton et al. 2013; Braiding et al. 2015; Rebolledo et al. 2016; Rebolledo et al. 2017), the beam size and velocity resolution of which are $\sim 35''$ and $\sim 0.09\ \text{km s}^{-1}$, respectively. The rms noise levels for the ^{12}CO and ^{13}CO ($J=1-0$) datasets are $\sim 4.0\ \text{K}$ and $\sim 1.9\ \text{K}$ per channel on the T_{mb} scale, respectively, at a velocity grid of $0.09\ \text{km s}^{-1}$.

2.2 NANTEN2

The ^{12}CO ($J=2-1$) data toward Gum 31 were obtained with the NANTEN2 4-m millimeter/sub-millimeter telescope at Atacama, Chile in 2015 October. The beam size of NANTEN2 at $\sim 230\ \text{GHz}$ corresponds to $\sim 90''$, and we adopted the on-the-fly (OTF) mapping mode with Nyquist sampling. The backend and frontend system and calibration are the same as in Paper I. A typical uncertainty in the intensity is $\sim 20\%$, and the typical rms noise level for the ^{12}CO ($J=2-1$) data is $\sim 0.3\ \text{K}$ per

channel on the T_{mb} scale at the velocity grid of 0.5 km s^{-1} .

3 Results

Figure 1(b) shows the ^{12}CO ($J=1-0$) integrated-intensity distributions (Mopra) with the velocity range from -35 to 10 km s^{-1} . It has a roughly ring-shaped structure, and the double or multiple O-type stars in HD 92206 has been identified (e.g., Mathys 1988; Maíz-Apellániz et al. 2004) at a location that is offset eastward from the center. We estimated that the maximum column density of the molecular gas is $1 \times 10^{23} \text{ cm}^{-2}$ and the total molecular gas mass (within the dotted square in Figure 1) is about $1.4 \times 10^5 M_{\odot}$ by using the same method as in Paper I.

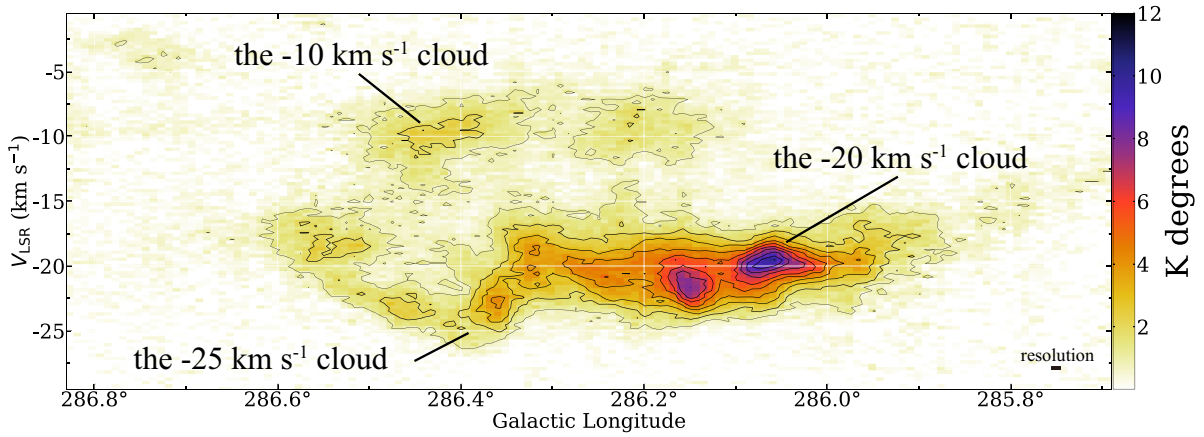
Figure 2 shows the $l-v$ diagrams of the ^{12}CO ($J=1-0$) toward Gum 31 with the integrated ranges (a) from $-0^{\circ}.4$ to $+0^{\circ}.2$, (b) from $-0^{\circ}.1$ to $+0^{\circ}.2$, and (c) from $-0^{\circ}.4$ to $-0^{\circ}.1$. In Figure 2(b), in the northern part, we detected two clouds separated in velocity and centered at ~ -20 and $\sim -10 \text{ km s}^{-1}$ (hereinafter called the -20 km s^{-1} cloud and the -10 km s^{-1} cloud, respectively). On the other hand, in Figure 2(c), there are two velocity components separated in velocity and centered at ~ -25 (hereinafter called the -25 km s^{-1} cloud) and $\sim -20 \text{ km s}^{-1}$ with a velocity gradient. In addition, there is also an intermediate velocity component in between.

Figure 3 shows the integrated-intensity ratios ^{12}CO ($J=2-1$)/ ^{12}CO ($J=1-0$) (hereinafter denoted by $R_{2-1/1-0}^{12}$) (color image) and the integrated-intensity distributions of the ^{12}CO ($J=1-0$) emission (contours) for the three clouds. The $R_{2-1/1-0}^{12}$ of the -25 km s^{-1} cloud and the -20 km s^{-1} cloud are high (>0.8) at the edge of the clouds, indicating that they are heated by the surrounding HII region in the same way as the cloud in the CNC. In contrast, the $R_{2-1/1-0}^{12}$ of the -10 km s^{-1} cloud is low (~ 0.4). For these reasons, it is probable that the former two are associated with the HII region, and the latter is not.

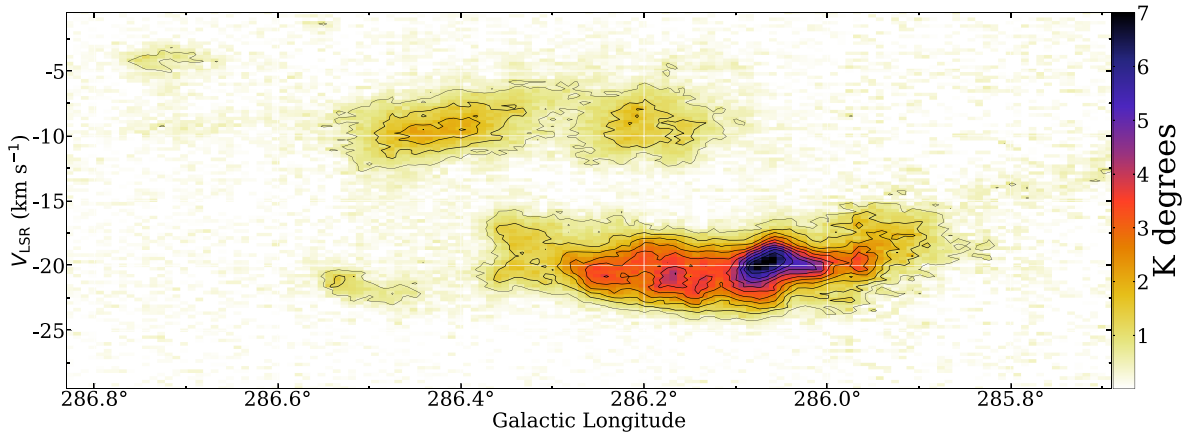
4 Discussion

The observations with Mopra and NANTEN2 have shown that the two CO clouds, the -25 km s^{-1} cloud and the -20 km s^{-1} cloud, are both associated with Gum 31. The molecular mass of the two are $4.9 \times 10^4 M_{\odot}$ (from -27 km s^{-1} to -21 km s^{-1}) and $2.3 \times 10^4 M_{\odot}$ (from -21 km s^{-1} to -15 km s^{-1}), respectively, within a radius of 15 pc centered on Gum 31. By tentatively assuming the most plausible viewing angle of the relative motion of the clouds to the line-of-sight is 60° (Fujita et al. 2021b), the relative velocity between the two is 10 km s^{-1} , which requires the total mass of $\frac{rv^2}{2G} = 1.7 \times 10^5 M_{\odot}$ to bind the two clouds gravitationally within 15 pc (where r and G are the distance between the two clouds and the gravitational constant, respectively). This is a factor of 2 larger than the total molecular

(a) $b = -0.4^\circ$ to $+0.2^\circ$



(b) $b = -0.1^\circ$ to $+0.2^\circ$



(c) $b = -0.4^\circ$ to -0.1°

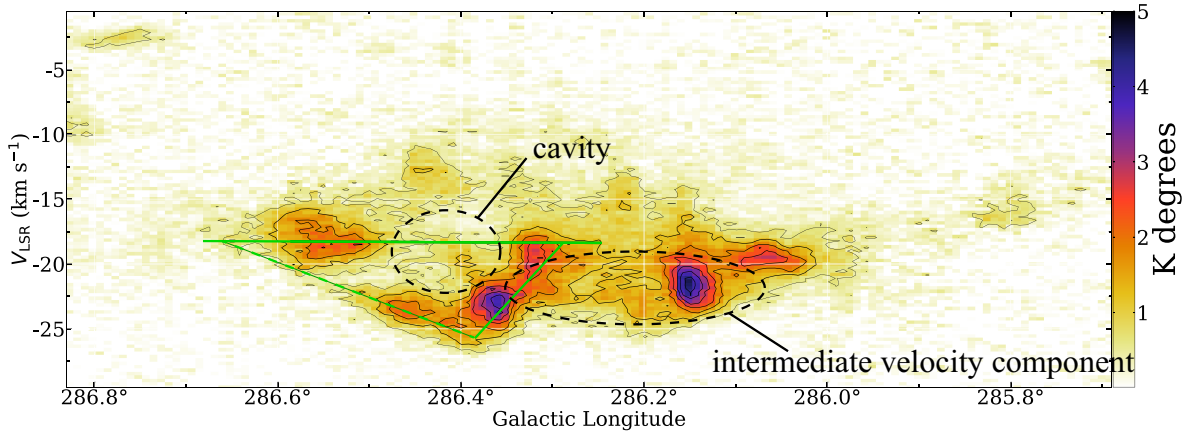


Fig. 2: (a) Galactic longitude – Velocity ($l-v$) diagram of the ^{12}CO ($J=1-0$) emissions integrated from -0.4° to $+0.2^\circ$. (b) The same as (a), but integrated from -0.1° to $+0.2^\circ$ (A in Figure 1(b)). (c) The same as (a), but integrated from -0.4° to -0.1° . (B in Figure 1(b))

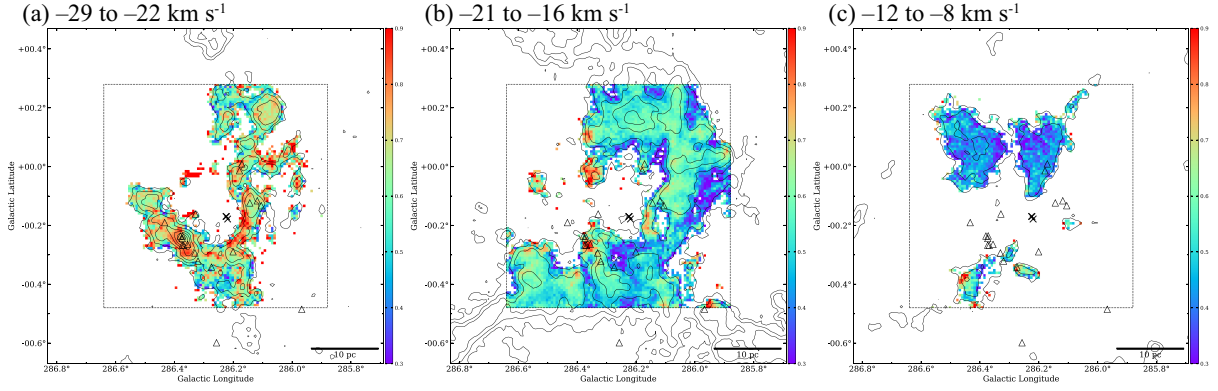


Fig. 3: The integrated-intensity ratio $^{12}\text{CO} (J=2-1)/^{12}\text{CO} (J=1-0)$ ($R_{2-1/1-0}^{12}$) map for the velocity range (a) from -29 km s^{-1} to -22 km s^{-1} , (b) from -21 km s^{-1} to -16 km s^{-1} , and (c) from -12 km s^{-1} to -8 km s^{-1} , respectively. The symbols are the same as in Figure 1.

mass of the two clouds derived, indicating that the coexistence of the two clouds cannot be understood as a gravitationally bound system. Therefore, the velocity structure of the molecular gas in Gum 31 is thought to be in the middle of or as a result of some dynamic event.

4.1 Expanding shell model

A possible explanation of the velocity components and the morphology of Gum 31 is the feedback effects from the exciting stars in HD 92206, such as the stellar wind, UV radiation, and pressure of expanding HII region. However, HD 92206 stars are offset from the center of the bubble-like structure of Gum 31. In addition, in Figure 2(a) we can not see clear expanding motion, namely an ellipse in the $p-v$ diagram, of the cloud either in the northern or the southern part of Gum 31. Figures 4(a)(b) shows the first moment of the $^{12}\text{CO} (J=1-0)$ emissions and the $^{13}\text{CO} (J=1-0)$ emissions, respectively, with a velocity range from -27 km s^{-1} to -15 km s^{-1} . It is clear that the insider cloud is blueshifted (the -25 km s^{-1} cloud) and the outsider is redshifted (the -20 km s^{-1} cloud). If the cloud is isotropically expanding, such a velocity gradient should not be seen. For these reasons, molecular gas in Gum 31 is likely to not have an expanding structure.

4.2 An Alternative: Cloud–cloud collision

Paper I suggests complex CCCs in the CNC. The existence of different velocity components, relatively weak CO emissions at intermediate velocities between two clouds (a bridge feature) in a $p-v$ diagram, and a complementary spatial distribution were reported as evidence of CCCs. The combination of the two characteristics of a bridge feature and a complementary spatial distribution made the

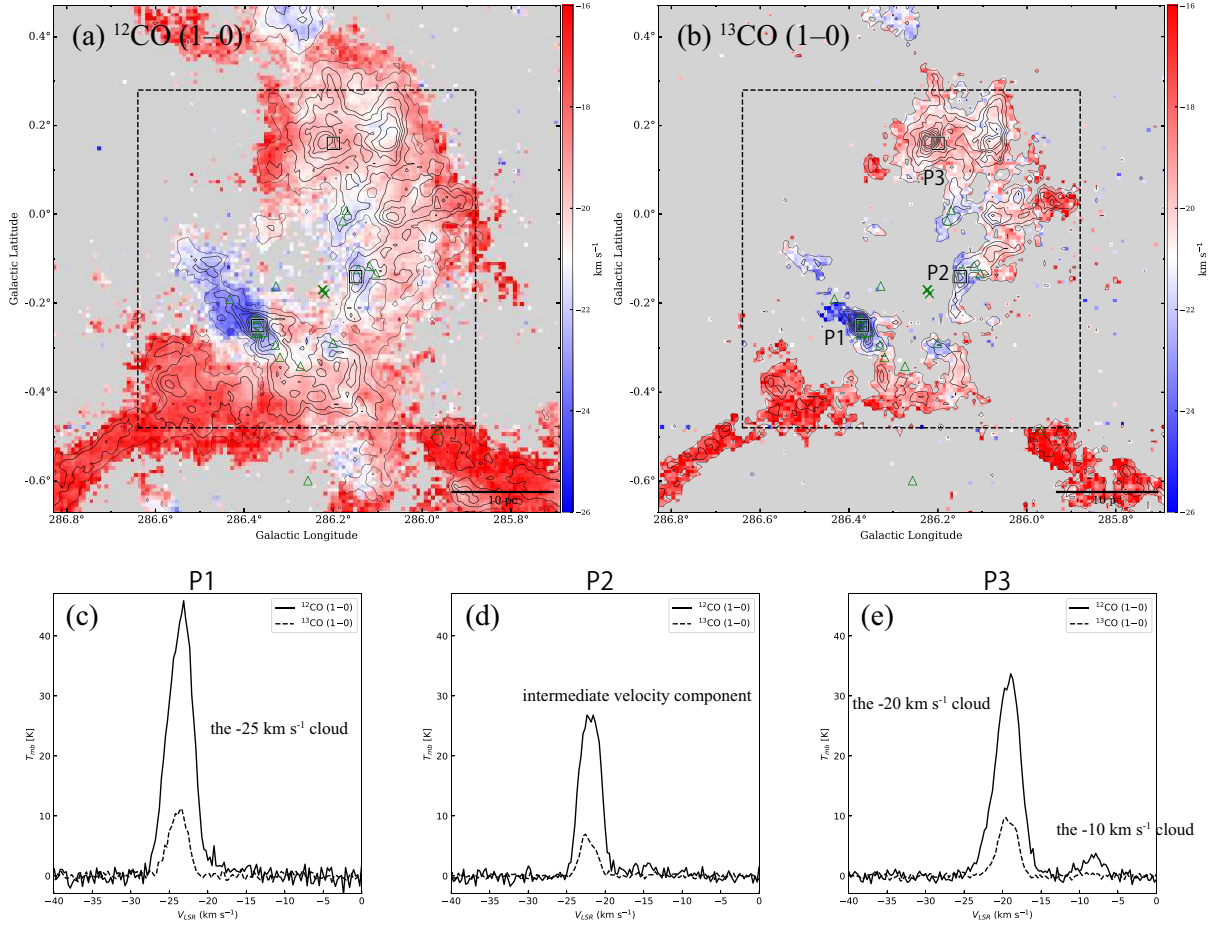


Fig. 4: (a) Map of the 1st moment of the ^{12}CO ($J=1-0$) emission between -27 km s^{-1} and -15 km s^{-1} . The contours show the moment 0 (integrated-intensity) of the ^{12}CO ($J=1-0$) emission. The contours are plotted every 25 K km s^{-1} from 25 K km s^{-1} ($\sim 10\sigma$). The symbols are the same as in Figure 1. (b) The same as (a), but for the ^{13}CO ($J=1-0$). (c–e) The spectra of the ^{12}CO ($J=1-0$) and the ^{13}CO ($J=1-0$) at the position P1, P2, and P3, respectively, shown by square makers.

p - v diagram V-shaped.

In Figure 2(c), we found that a V-shape structure in the l - v diagrams can be seen. In addition, it was found that the two velocity components show complementary spatial distributions (Figure 5). These morphology and velocity structures are very similar to the numerical simulations conducted by e.g., Habe & Ohta (1992), Takahira et al. (2014), and Haworth et al. (2015). That is, a small cloud (the -25 km s^{-1} cloud) collided with the large cloud (the -20 km s^{-1} cloud) at supersonic velocity from the eastern side, and formed a cavity. The small cloud has a larger mass than the large cloud ($4.9 \times 10^4 M_{\odot}$ and $2.3 \times 10^4 M_{\odot}$, respectively). It is considered that the initial density of the small cloud was higher than that of the large cloud, if we assume that their thickness on the line-of-sight direction are about the same. These conditions are similar to the numerical simulation conducted by Takahira et al. (2014). After the collision, the two were merged in the interface layers, and turbulence was predominant due to strong compression, forming a molecular cloud core that formed massive stars in HD 92206. Furthermore, the collision scenario can interpret the offset of HD 92206 from the center of Gum 31 seen in Figure 1(a) and the first moment and spectra of the molecular gas in Figures 4. Figure 6 shows a sketch diagram of this collision scenario in Gum 31. Such a CCC scenario has also been proposed for RCW 120 (Torii et al. 2015) and N4 (Fujita et al. 2019), which have a similar appearance to Gum 31. The time scale of the collision is roughly estimated as $\sim 10 \text{ pc} / (5 \text{ km s}^{-1} \times 2) \sim 1 \text{ Myr}$ from the size of the cavity and the velocity separation of the molecular cloud, with the assumption that the angle between the line of sight and the collision axis is 60° . There is no large contradiction between this collision time scale and the young age of the cluster NGC 3324 ($< 3 \text{ Myr}$, Carraro et al. 2001).

We conclude that the massive star formation of the CNC and Gum 31 were triggered by multiple CCCs and a CCC, respectively, because the CCC scenario in Gum31 is consistent with Paper I results in terms of the collision timescale and the collision direction. It is considered that the source that caused the multiple CCCs in the CNC and Gum31 is possibly the same. This picture is similar to the star formation history in W51 (Fujita et al. 2021b), which has similar star formation activity (dozens of O-type stars) to Carina. In addition, our results support the proposal that Gum 31 is part of the CNC (Ohlendorf et al. 2013).

For the YSOs (triangle markers in Figure 1(a)), it cannot be determined by this study whether the formation was triggered by the collision or triggered by the feedback of stars in Gum 31 as suggested by Cappa et al. (2008). In the future, it will be possible to discuss this by e.g., detailed measurement of their ages.

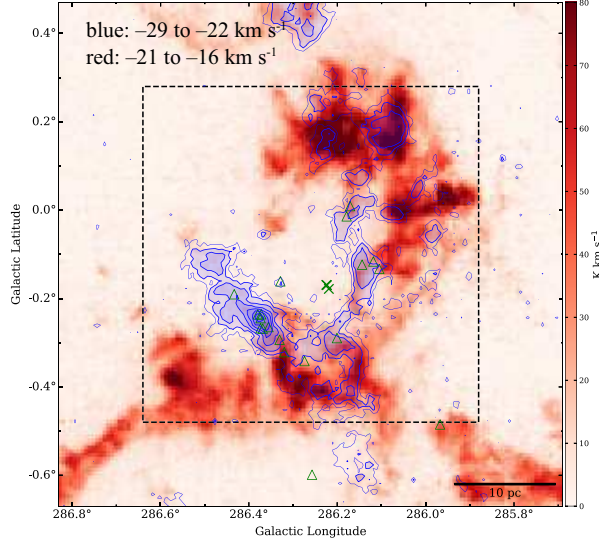


Fig. 5: The red and blue show the integrated-intensity distributions of the ^{12}CO ($J=1-0$) emissions toward Gum 31. The each integrated velocity ranges are shown in the top left corner of the figure. The contour levels are 8, 16, 32, 64, 96, 128, and 160 K km s^{-1} . The symbols are the same as in Figure 1.

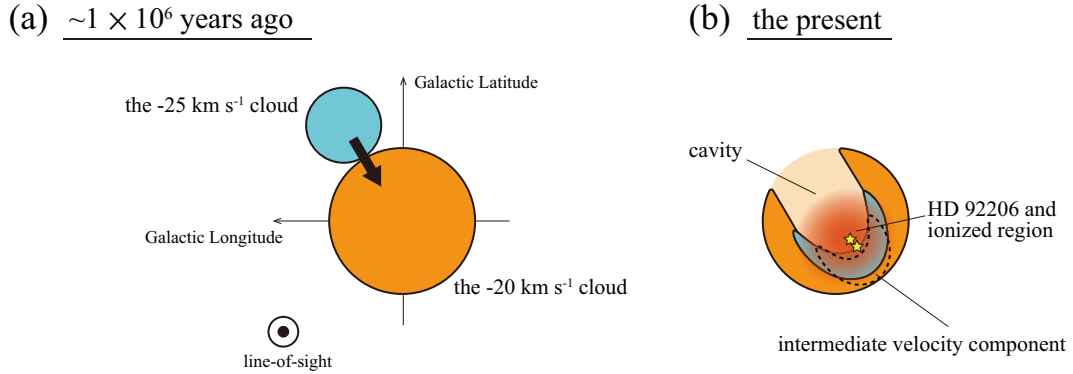


Fig. 6: A sketch diagram of the cloud–cloud collision scenario in Gum 31.

5 Summary

1. We analysed the ^{12}CO ($J=1-0$), ^{13}CO ($J=1-0$) (Mopra), and ^{12}CO ($J=2-1$) (NANTEN2) emission lines toward Gum 31, and found the discrete three molecular clouds at velocities -25 , -20 , and -10 km s^{-1} .
2. The -25 km s^{-1} cloud and the -20 km s^{-1} cloud are associated with Gum 31, because their ^{12}CO ($J=2-1$)/ ^{12}CO ($J=1-0$) intensity ratios are high. In addition, these clouds show the observational signatures of a CCC as same as the clouds in the CNC. In addition, their morphology and velocity structures are very similar to the numerical simulations conducted by the previous studies.
3. We propose a scenario that the -25 km s^{-1} cloud and the -20 km s^{-1} cloud were collided and

triggered the formation of the massive stars in Gum 31. This CCC scenario can explain the offset of the stars from the center and the morphology of Gum 31 simultaneously. We estimate the timescale of the collision to be ~ 1 Myr by using the path length of the collision and the assumed velocity separation. This is roughly consistent with that of the CCCs in the CNC estimated in our previous study, which support that Gum 31 is part of the CNC.

Acknowledgments

We are deeply grateful to the financial support by Grants-in-Aid for Scientific Research (KAKENHI) of the Japanese society for the Promotion of Science (JSPS; grant numbers 15K17607, 17H06740, and 18K13580), and we would like to thank the all members of the NASA, Mopra, and NANTEN2 for providing the data. Also, we want to thanks Astropy (Astropy Collaboration et al. 2013) and APLpy (Robitaille & Bressert 2012) development team for data analysis.

References

- Allen, D. A., & Hillier, D. J. 1993, *Proceedings of the Astronomical Society of Australia*, 10, 338
- Astropy Collaboration, Robitaille, T. P., Tollerud, E. J., et al. 2013, *A&A*, 558, A33
- Barnes, P. J., Yonekura, Y., Ryder, S. D., et al. 2010, *MNRAS*, 402, 73. doi:10.1111/j.1365-2966.2009.15890.x
- Braiding, C., Burton, M. G., Blackwell, R., et al. 2015, *PASA*, 32, e020
- Burton, M. G., Braiding, C., Glueck, C., et al. 2013, *PASA*, 30, e044
- Cappa, C., Niemela, V. S., Amorín, R., et al. 2008, *A&A*, 477, 173. doi:10.1051/0004-6361:20067028
- Carraro, G., Patat, F., & Baumgardt, H. 2001, *A&A*, 371, 107. doi:10.1051/0004-6361:20010307
- Churchwell, E., Povich, M. S., Allen, D., et al. 2006, *ApJ*, 649, 759
- Churchwell, E., Watson, D. F., Povich, M. S., et al. 2007, *ApJ*, 670, 428
- Enokiya, R., Sano, H., Hayashi, K., et al. 2018, *PASJ*, 70, S49
- Fujita, S., Torii, K., Tachihara, K., et al. 2019, *ApJ*, 872, 49
- Fujita, S., Tsutsumi, D., Ohama, A., et al. 2021a, *PASJ*, 73, S273. doi:10.1093/pasj/psaa005
- Fujita, S., Torii, K., Kuno, N., et al. 2021b, *PASJ*, 73, S172. doi:10.1093/pasj/psz028
- Fujita, S., Sano, H., Enokiya, R., et al. 2021c, *PASJ*, 73, S201. doi:10.1093/pasj/psaa078
- Fukui, Y., Ohama, A., Hanaoka, N., et al. 2014, *ApJ*, 780, 36
- Fukui, Y., Torii, K., Ohama, A., et al. 2016, *ApJ*, 820, 26
- Fukui, Y., Tsuge, K., Sano, H., et al. 2017, *PASJ*, 69, L5
- Fukui, Y., Tokuda, K., Saigo, K., et al. 2019, *ApJ*, 886, 14
- Fukui, Y., Habe, A., Inoue, T., et al. 2021, *PASJ*, 73, S1. doi:10.1093/pasj/psaa103
- Furukawa, N., Dawson, J. R., Ohama, A., et al. 2009, *ApJL*, 696, L115

Habe, A., & Ohta, K. 1992, PASJ, 44, 203

Hanaoka, M., Kaneda, H., Suzuki, T., et al. 2019, PASJ, 71, 6. doi:10.1093/pasj/psy126

Haworth, T. J., Tasker, E. J., Fukui, Y., et al. 2015, MNRAS, 450, 10

Hayashi, K., Sano, H., Enokiya, R., et al. 2018, PASJ, 70, S48

Kohno, M., Torii, K., Tachihara, K., et al. 2018, PASJ, 70, S50

Mathys, G. 1988, A&AS, 76, 427

Maíz-Apellániz, J., Walborn, N. R., Galué, H. Á., et al. 2004, ApJS, 151, 103. doi:10.1086/381380

Nishimura, A., Minamidani, T., Umemoto, T., et al. 2018, PASJ, 70, S42. doi:10.1093/pasj/psx149

Ohama, A., Dawson, J. R., Furukawa, N., et al. 2010, ApJ, 709, 975

Ohlendorf, H., Preibisch, T., Gaczkowski, B., et al. 2013, A&A, 552, A14. doi:10.1051/0004-6361/201220218

Rebolledo, D., Burton, M., Green, A., et al. 2016, MNRAS, 456, 2406

Rebolledo, D., Green, A. J., Burton, M., et al. 2017, MNRAS, 472, 1685

Robitaille, T., & Bressert, E. 2012, Astrophysics Source Code Library, ascl:1208.017

Sano, H., Enokiya, R., Hayashi, K., et al. 2018, PASJ, 70, S43

Sano, H., Tsuge, K., Tokuda, K., et al. 2021, PASJ, 73, S62. doi:10.1093/pasj/psaa045

Smith, N. 2006, ApJ, 644, 1151

Takahira, K., Tasker, E. J., & Habe, A. 2014, ApJ, 792, 63

Tokuda, K., Fukui, Y., Harada, R., et al. 2019, ApJ, 886, 15

Torii, K., Hasegawa, K., Hattori, Y., et al. 2015, ApJ, 806, 7

Torii, K., Hattori, Y., Hasegawa, K., et al. 2017a, ApJ, 835, 142

Torii, K., Hattori, Y., Hasegawa, K., et al. 2017b, ApJ, 840, 111

Torii, K., Fujita, S., Matsuo, M., et al. 2018b, PASJ, 70, S51

Torii, K., Hattori, Y., Matsuo, M., et al. 2021, PASJ, 73, S368. doi:10.1093/pasj/psy098

Walborn, N. R. 1982, AJ, 87, 1300. doi:10.1086/113216

Yonekura, Y., Asayama, S., Kimura, K., et al. 2005, ApJ, 634, 476